

# FRAMEWORK VALIDATION FOR TESTING BUILD UNIFORMITY IN ADDITIVELY MANUFACTURED 17% CHROMIUM 4% NICKEL STAINLESS STEEL

Julianna Posey<sup>1</sup>, Michael Duffy<sup>1</sup>, Caroline Vail<sup>2</sup>, Marc Zupan<sup>1</sup>

<sup>1</sup>University of Maryland, Baltimore County, Department of Mechanical Engineering

Baltimore, MD, USA

<sup>2</sup>Naval Surface Warfare Center, Carderock Division

Carderock, MD, USA

## ABSTRACT

For additive manufacturing (AM) to meet industrial needs for next-generation marine vessels, the impact of processing parameters, geometry, and material performance must be defined. Specifically, precipitation hardenable stainless steels have been identified for research due to the capability for increased corrosion resistance and strength. Alloyed 17% Chromium - 4% Nickel (17-4 PH) thin fin structures of three thicknesses and four build angles and zig-zag structures of four width reductions were manufactured using a EOS M290 powder bed fusion AM system. This work characterizes and defines relevant processing parameters and manufacturing techniques that cause differences in component and material performance. Surface roughness is measured at upskin and downskin surfaces at different build angles. Vickers hardness testing is explored with respect to build geometry. Recommendations are provided for a comparative analysis.

**Keywords:** additive manufacturing, 17-4 precipitation hardened stainless steel, surface roughness, hardness, powder bed fusion, metal

## 1. INTRODUCTION

Metal additive manufacturing (AM) has been increasingly utilized in operations that require cost-effective solutions for three-dimensional metal components [1]. Through this process, metal components can be digitally designed and are available on-demand in a variety of materials. Designers of next-generation marine vehicles have an interest in relying on metal AM to produce highly intricate and weight-critical replacement parts for systems that are past production [2]. However, the inherently heterogeneous layer-by-layer build process currently results in a variety of discontinuities throughout the as-built state of a component. Anomalies can be caused by an assortment of variables, including manufacturing processing parameters, material selection, geometry, and machine type [2]. To understand metal AM and establish this process in industrial manufacturing, researchers must define the linkages of these defects to the material and component characteristics, responses, and behaviors.

*Copyright 2021. Used by the Society of the Advancement of Material and Process Engineering with permission.*

*SAMPE neXus Proceedings. Virtual Event, June 29 – July 1, 2021.  
Society for the Advancement of Material and Process Engineering – North America.*

This research examines components constructed through the powder bed fusion (PBF) metal AM process. For PBF, operations occur within a preheated chamber filled with an inert gas [3]. A directed laser beam selectively fuses a cross-sectional slice of the component model onto a layer of powder that is spread evenly across a preheated substrate base plate [4]. When printing a slice in a single layer, the laser first fuses the outline of the area, which is defined as the contour pass. The laser will then fill in the interior of the area through cross-hatching. This process is repeated for each layer of the component, with the machine recoating the powder layer and the laser selectively melting the next layer. As the component is built within the powder bed, small weld beads form the structure of the component and interact with the previously melted layers [4, 5]. Once the component is fully fused, it is removed from the powder bed and prepared for any necessary post-processing. Studies from Meredith et. al and Murr et. al have observed the chemical composition of 17% chromium 4% nickel precipitation hardenable stainless steel (17-4 PH SS) powder in PBF AM environments. The literature identifies that while composition is influenced by the atomization of the powder feedstock, the resulting chemical composition of the PBF manufactured component remains within the specified range for 17-4 stainless steel [6, 7].

### 1.1 Study Framework

For this work, alloyed 17-4 PH SS powder was selected and qualified for use by a vendor. This specific steel is of significant interest for marine applications due to its high tensile strength and resistance to corrosion. A build plate that consists of different geometric structures was designed and fabricated, as shown in Figure 1. On the build plate, there are four quadrants consisting of two quadrant designs that are printed twice onto a base plate in different orientations with respect to the powder recoater direction. These structures were selected to influence diverse component characteristics and a complex thermal history. The build plate was designed so each layer took the same time to produce. In PBF systems, surfaces at angles to the base plate have powder particles that partially melt at the interface between the fully consolidated component and the surrounding loose powder bed. These surfaces are defined as upskin or downskin surfaces.

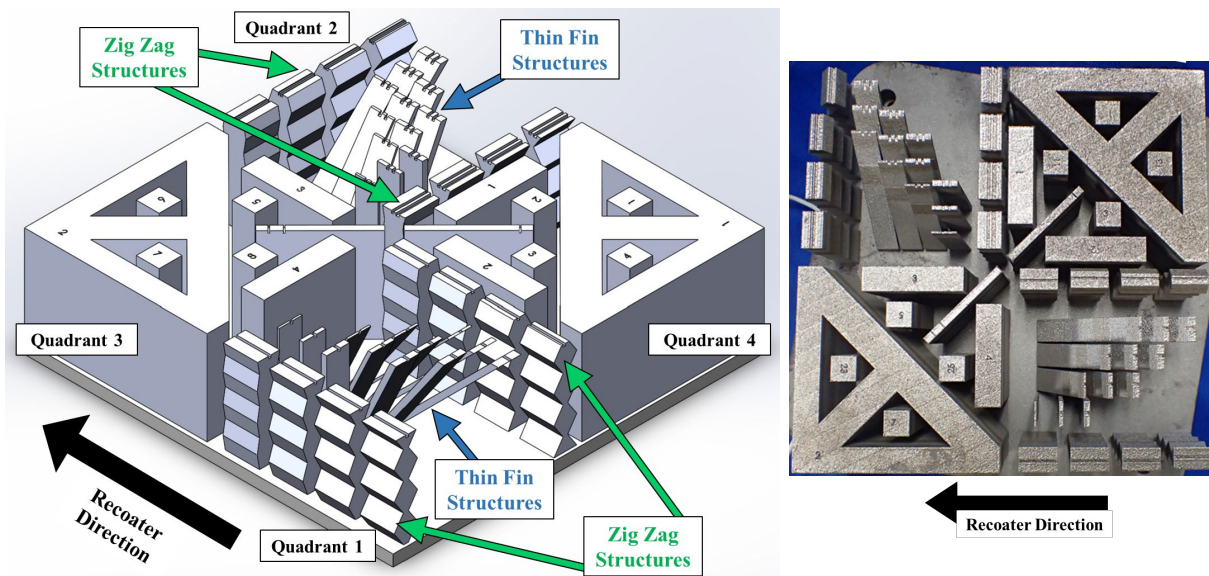


Figure 1. Build plate footprint with highlighted structures utilized for this work [8].

This manuscript is a part of a larger repeatability study that aims to establish variation between different PBF AM systems over time and make comparisons over multiple makes and models of PBF systems. The purpose of this manuscript is to assist in developing the testing process for the larger study by understanding how characteristics change over the thin fin and zig zag structures located in Quadrants 1 and 3, as shown in Figure 1. This body of work will describe the research that determined the requirements for evaluating the surface roughness and hardness.

## 2. TEST METHODS

The material in this work was built using pre-alloyed and argon atomized 17-4 PH SS powder. The AM process was conducted using an EOS M290 system with an argon environment and the standard machine specifications and manufacturer-recommended machine processing parameters for 17-4 PH SS powder. Components shown in Figure 2 were removed from the base plate for testing and were not heat-treated, meaning the material is non-precipitation hardened.

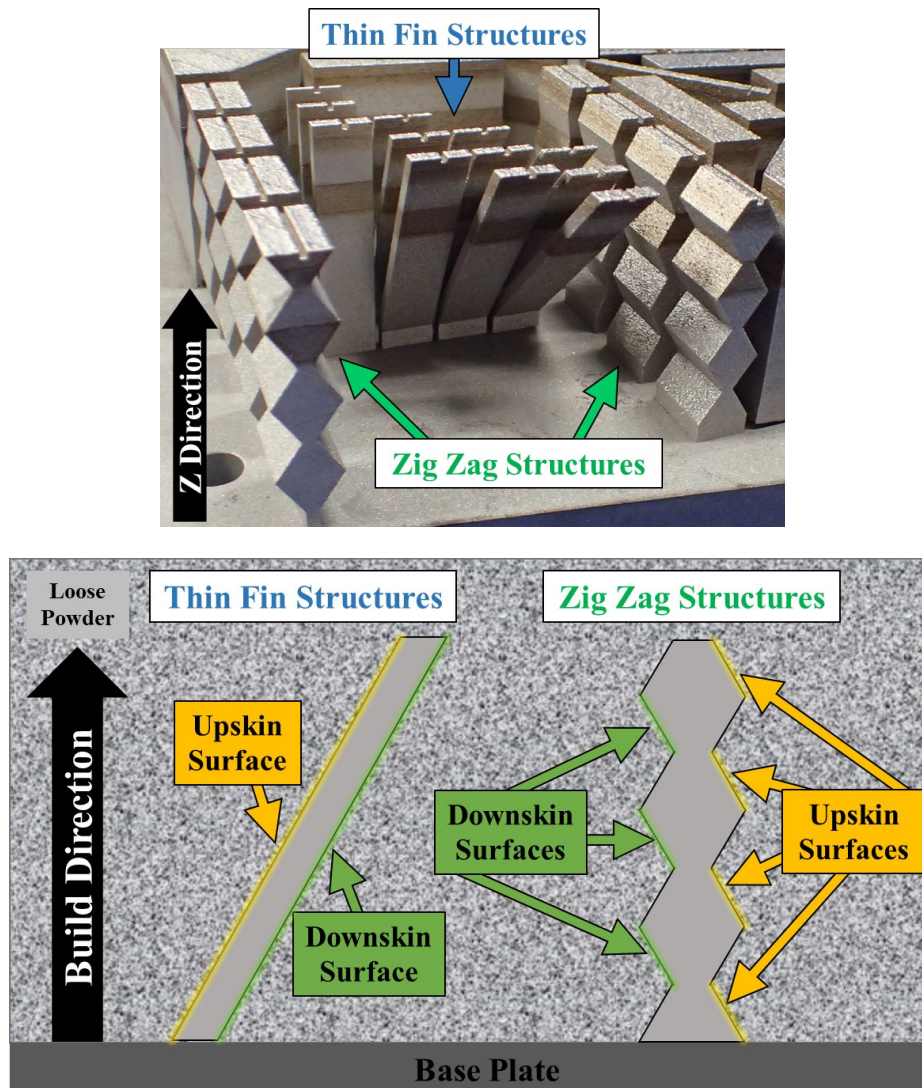


Figure 2. Upskin and downskin surfaces identified on thin fin and zig zag structures [8].

Twelve thin fin structures and eight zig zag structures from Quadrant 1 of the build plate, shown in Figure 3, are characterized by evaluating the surface roughness and hardness within the component. Thin fin structures have thicknesses of 1mm, 2mm, and 3mm, and are built at angles of 90°, 65°, 55°, and 45° with respect to the base plate. Zig zag structures are designed with a maximum width of 15 mm that is reduced three times throughout the build height by 20%, 40%, 60%, or 80% of the maximum width, generating multiple upskin and downskin surfaces. The zig zag structures are also built with either a wide base of 15 mm or a narrow base corresponding to the individual structure's width reduction.

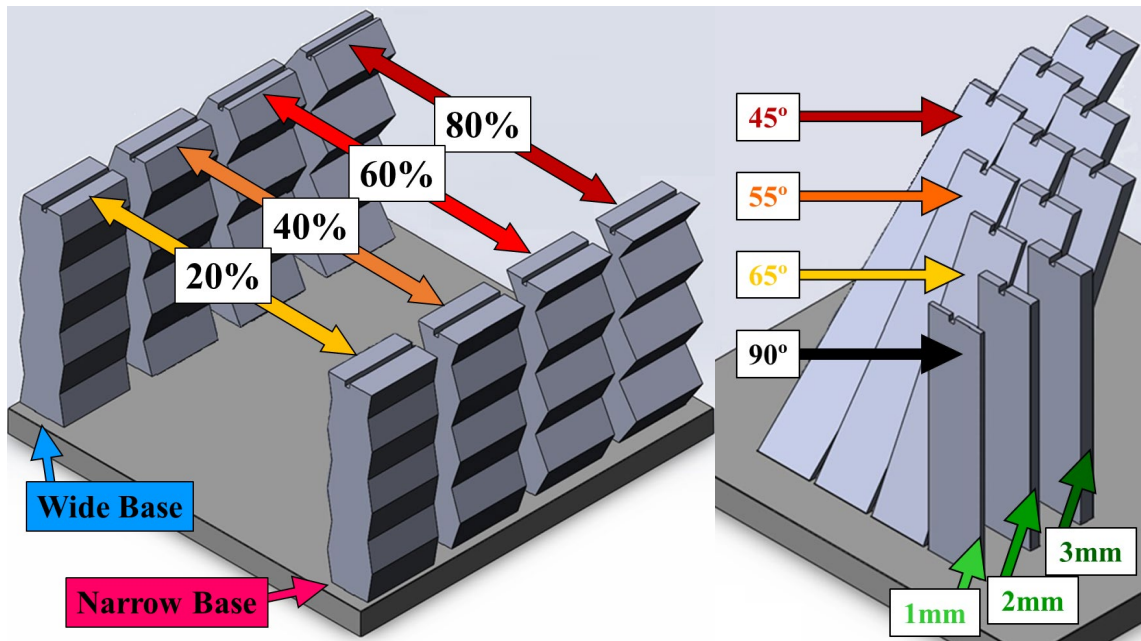


Figure 3. Thin fin and zig zag structures on one quadrant with defined geometries [8].

The following sections will describe the characterization methods and tools used to determine the surface roughness and hardness of the thin fin and zig zag structures.

## 2.1 Surface Roughness Testing

Surface roughness measurements were completed using both optical and physical profilometry methods. The Ra roughness parameter measures the average of the absolute deviation from the mean height. This value was reported as a baseline understanding of how roughness varies over different geometries [9]. To determine how roughness varies over a single upskin or downskin surface on the thin fin structures, a Keyence VK-X1000 3D Laser Scanning Confocal Microscope was used to examine nine locations on both upskin and downskin surfaces. Measurements were examined over a nominally 750  $\mu\text{m}$  x 500  $\mu\text{m}$  area using a 20X magnification, as shown in Figure 4. Scan locations were completed at depth intervals of 3.125 mm and at the build heights of 10 mm, 27 mm, and 45 mm. This strategy is utilized to examine locational roughness variations across different build heights and depths within the component and qualitatively evaluate features in the physical topography and texture of each surface.

For the zig zag structures, the confocal microscope was utilized to examine how roughness varies over multiple different surfaces within the height of the build. Using the same measurement parameters, twelve measurements were completed on each zig zag structure for a total of six upskin and six downskin measurements, as shown in Figure 5.

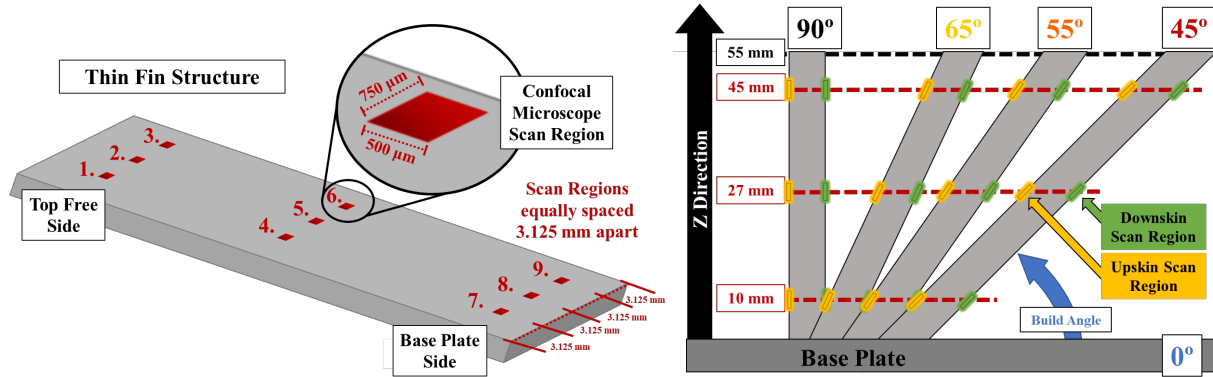


Figure 4. Locations of optical measurements on thin fin structure surfaces [8].

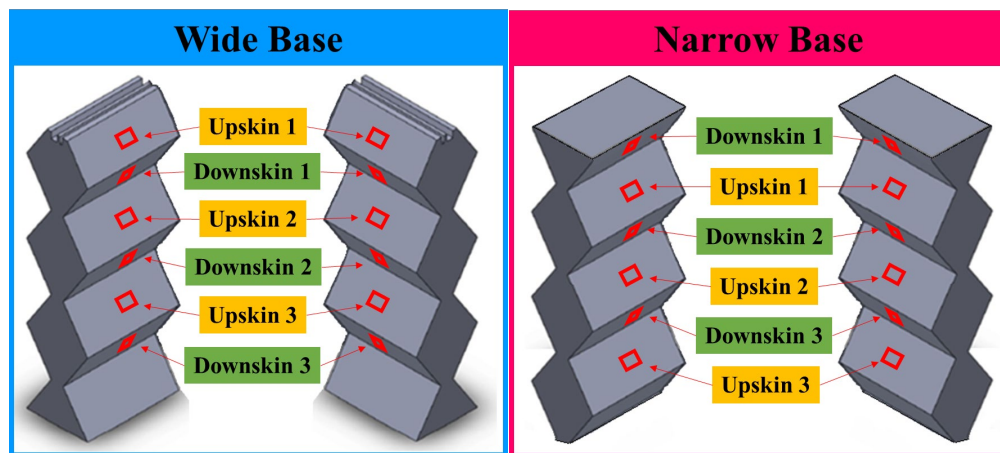


Figure 5. Locations of optical measurements on zig zag structure surfaces [8].

A Mitutoyo Surftest SJ-210 Surface Roughness Tester (portable stylus) was used to perform 12.5 mm physical profile section measurements on each upskin and downskin surface on the thin fin structures, as shown in Figure 6. This tool was utilized to examine its applicability to the larger study, since a significant benefit of measuring using the stylus is its speed, ease of use, and maneuverability. The ISO 4288 standard for non-periodic profiles was used to select the cutoff length ( $\lambda_c$ ) of 2.5 mm [10, 11].



Figure 6. Profile measurement location for thin fin structure surfaces [8].

## 2.2 Vickers Hardness Testing

The Vickers Hardness testing process was utilized to report locational microhardness data on thin fin and zig zag structures. A Phase II 900-391 Micro Vickers Hardness Tester and iVision measuring software was used to complete the measurements. In accordance with ASTM E92-82 testing procedures, a force of 4.9 N was used as the indentation load over a 15 second time frame [12, 13]. To prepare the structures for hardness testing, a 2.54 mm thick slice on the free edge of each thin fin structure and on the free face of each zig zag structure was sliced off using a Fanuc Alpha OiE wire electric discharge machine, as shown in Figures 7 and 8.

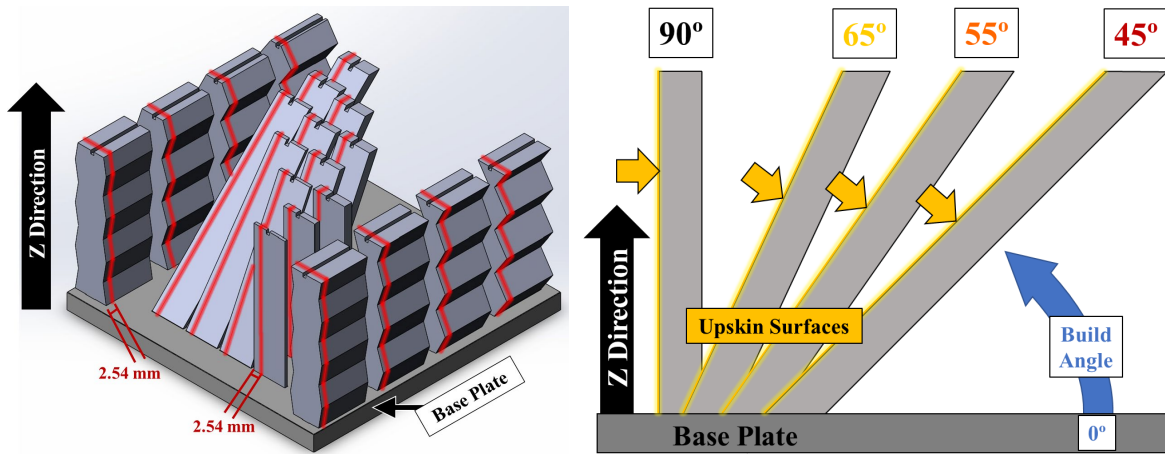


Figure 7. Diagram of slices removed from bulk thin fin structures [8].

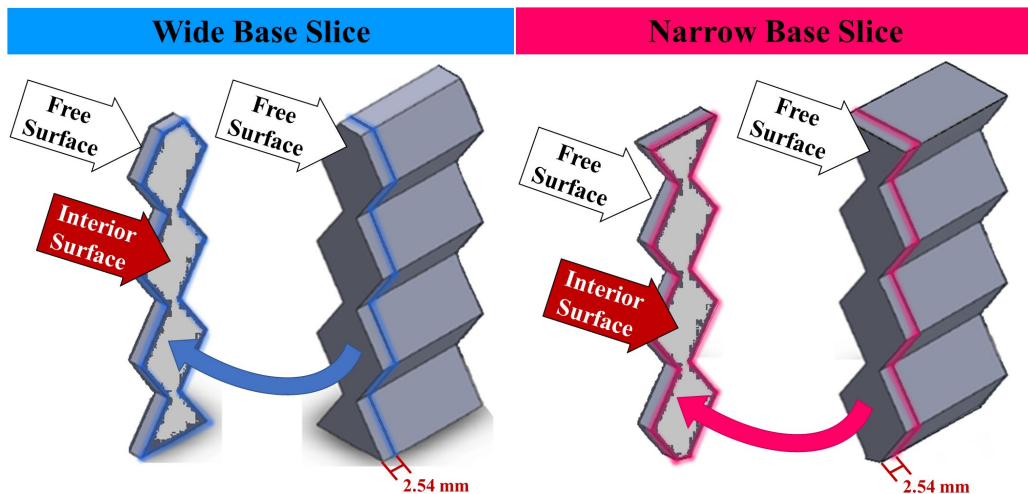


Figure 7. Diagram of slices removed from bulk zig zag structures [8].

The upskin surfaces on the bulk of the thin fin structures and the interior sliced surface of the zig zag structure slices were prepared for hardness testing using standard metallographic methods. Surfaces were polished with silicon carbide (SiC) polishing sheets and water lubrication, proceeding through 180, 320, 400, 600, 800, and 1200 grit papers. Final polishing was completed with a 0.05  $\mu\text{m}$  colloidal silica suspension and a synthetic velvet cloth.

Hardness testing methodology consisted of three rows of individual indents spaced 0.3 mm apart. This enabled interspersed measurements throughout the weld beads. For the thin fin structures, indents were conducted at the build heights of 10 mm, 27 mm, and 45 mm, and were directed from the sliced edge (Figure 7) to the free edge, as shown in Figure 8. For the zig zag structures, indentation rows were located at the build heights of 20 mm, 38 mm, and 56 mm. This meant that wide base zig zag structures were measured at the locations where width was maximized, and narrow base zig zag structures were measured at the locations where width was minimized. This is shown in Figure 9.

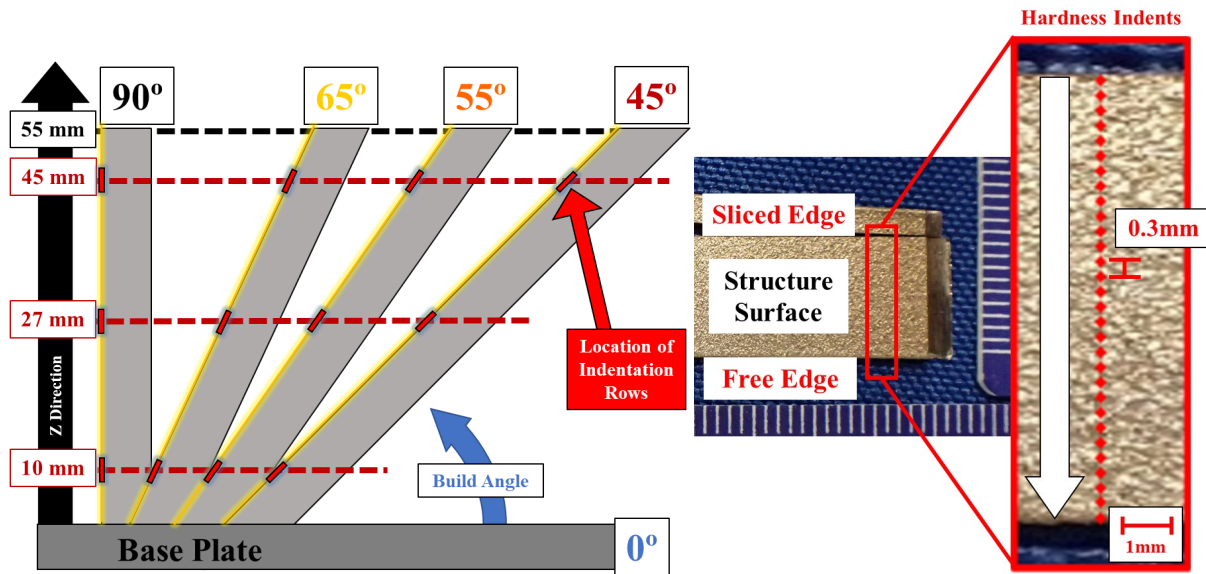


Figure 8. Hardness testing locations for thin fin structures and indentation methodology [8].

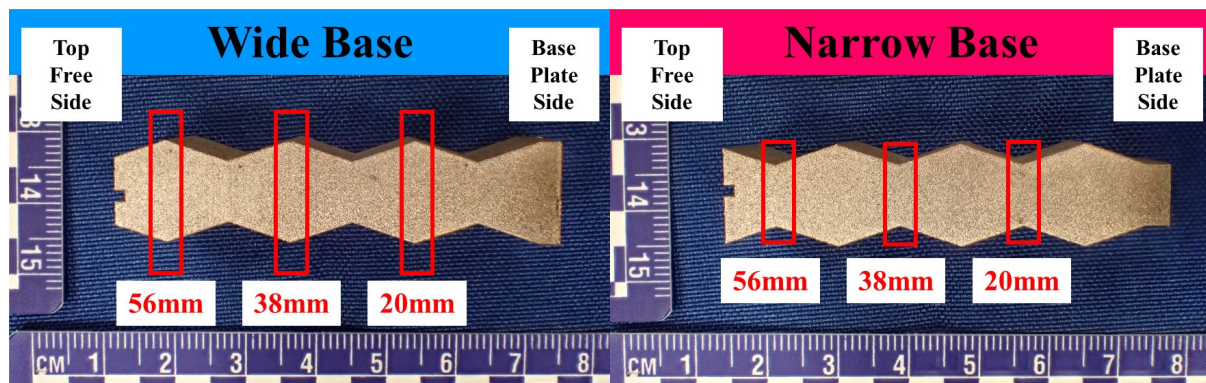


Figure 9. Hardness testing locations for zig zag structures [8].

### 3. RESULTS

#### 3.1 Surface Roughness Results

Figure 12 plots the optical surface roughness  $R_a$  measurements at the three build heights of 10 mm, 27 mm, and 45 mm for the upskin and downskin surfaces on the 90°, 65°, 55°, and 45° angled

thin fin structures at each of the three thicknesses. The coefficient of variation, defined in Equation 1, is a statistical tool used to examine the dispersion of data around the mean of a data set.

$$CV = \frac{\text{Standard Deviation}}{\text{Mean}} * 100 \quad \text{Equation 1}$$

Figure 13 plots the coefficient of variation across the 1mm, 2mm, and 3mm samples at each of the nine sample locations defined in Figure 4.

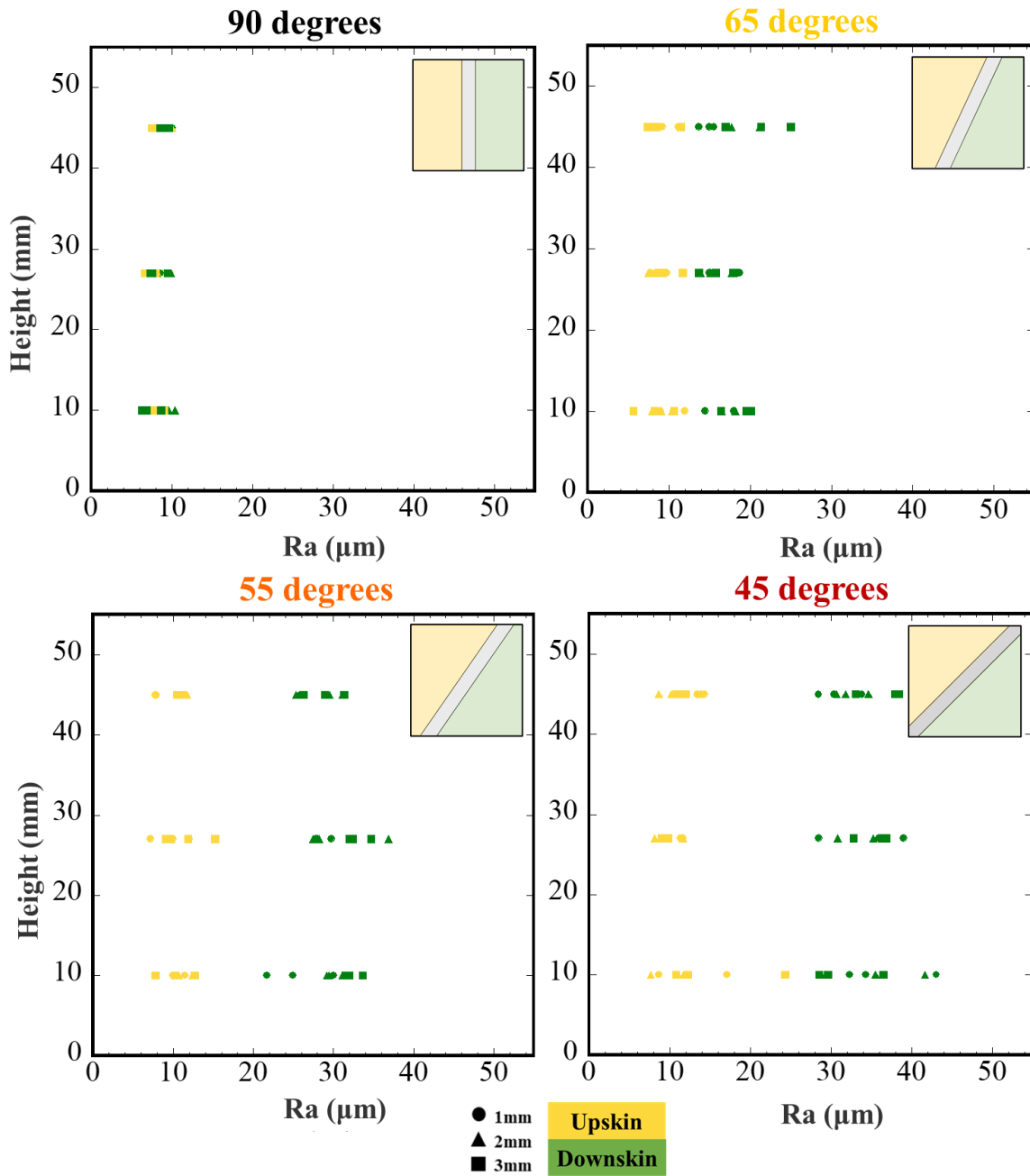


Figure 12. Optical roughness measurements at three heights for the thin fin structures [8].

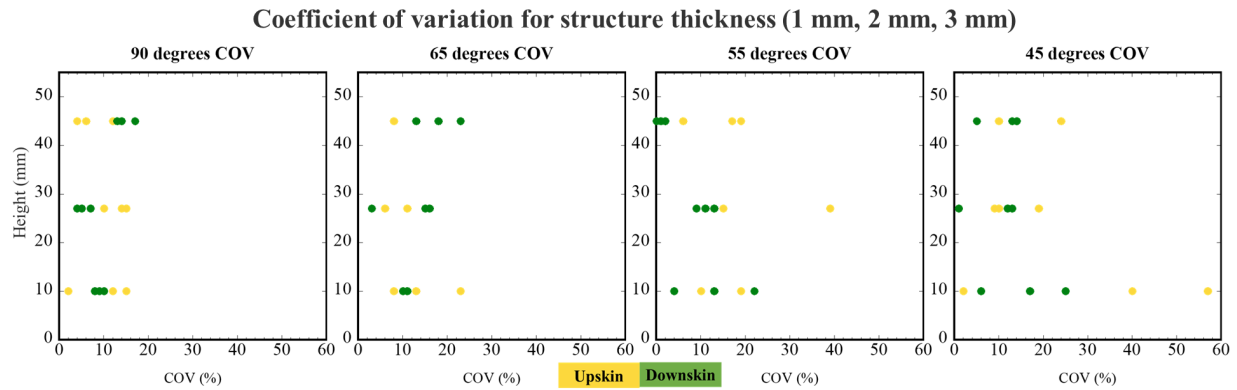


Figure 13. Coefficient of variation analysis for thin fin structures [8].

Roughness values remain consistent across the three thicknesses shown. A decrease in angle results in an increase in roughness and measurement variability, with the coefficient of variation increasing in range from 0-17% to 0-58%. However, qualitative inspection reveals greater concentrations of unmelted particles on downskin surfaces that increase in prevalence as the angle decreases. Upskin surfaces have interspersed partially melted particles that decrease in prevalence with a decrease in build angle. These features are shown in Figure 14 and explain the increased range of coefficient of variation values for upskin surfaces, as the dispersal of single-point powder particles cause inconsistencies in the upskin surface. From this analysis, roughness is not shown to vary due to structure thickness, structure height, or location along the width of the structure.

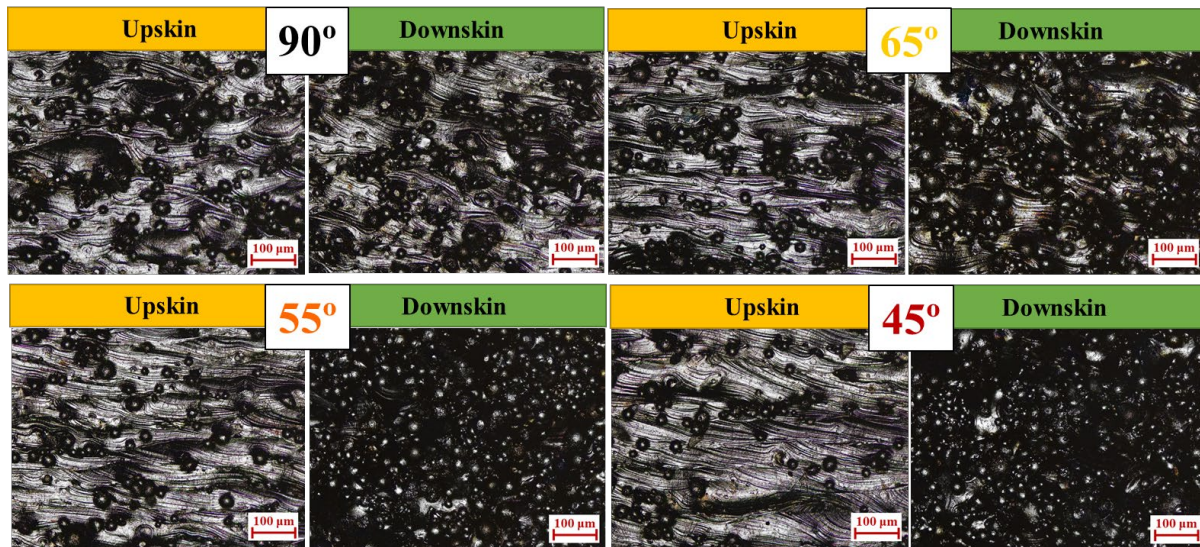


Figure 14. Surface roughness characteristics for upskin and downskin thin fin structures [8].

For the zig zag structures, a similar trend is found in the optical surface roughness measurements. Figure 15 shows how a greater width reduction (and thus a decreasing or steeper build angle) results in an overall larger roughness variability and an increase in roughness on the downskin surfaces. The coefficient of variation of the set of six upskin and six downskin surfaces on each zig zag structure is calculated and shown in Figure 16. Like the thin fin structures, a decrease in build angle for zig zag structures results in a higher roughness variation for upskin surfaces.

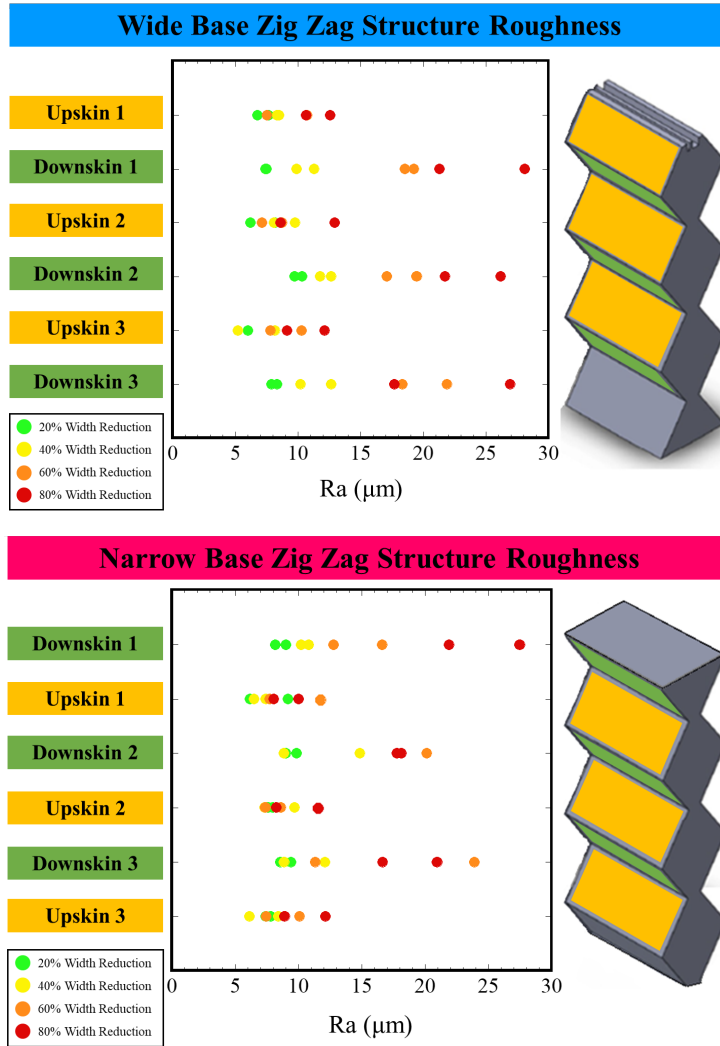


Figure 15. Zig zag structure roughness values plotted with respect to height in the build [8].

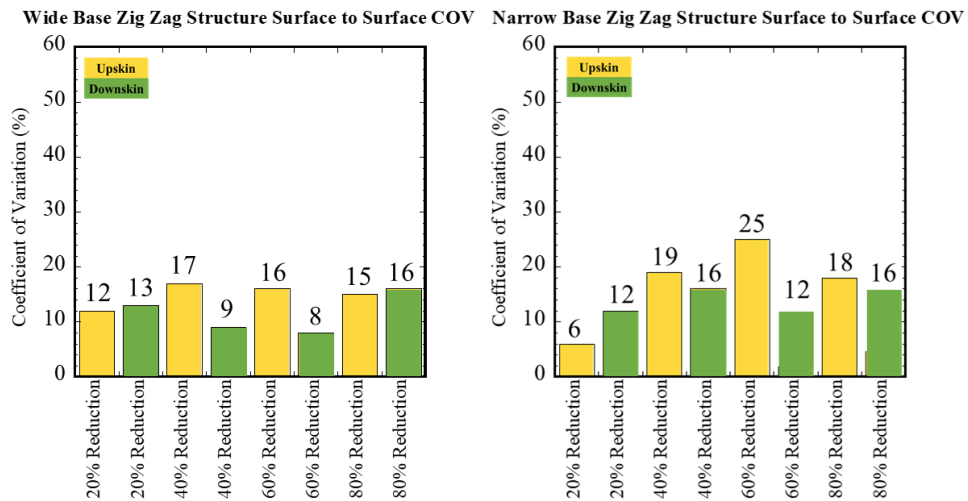


Figure 16. Coefficient of variation for upskin and downskin surfaces on zig zag structures [8].

The roughness of the thin fin structures evaluated using the stylus revealed similar results, as shown in Figure 17. Decreasing the build angle results in an increased surface roughness, and the downskin surface will increase at a greater magnitude than the upskin surface.

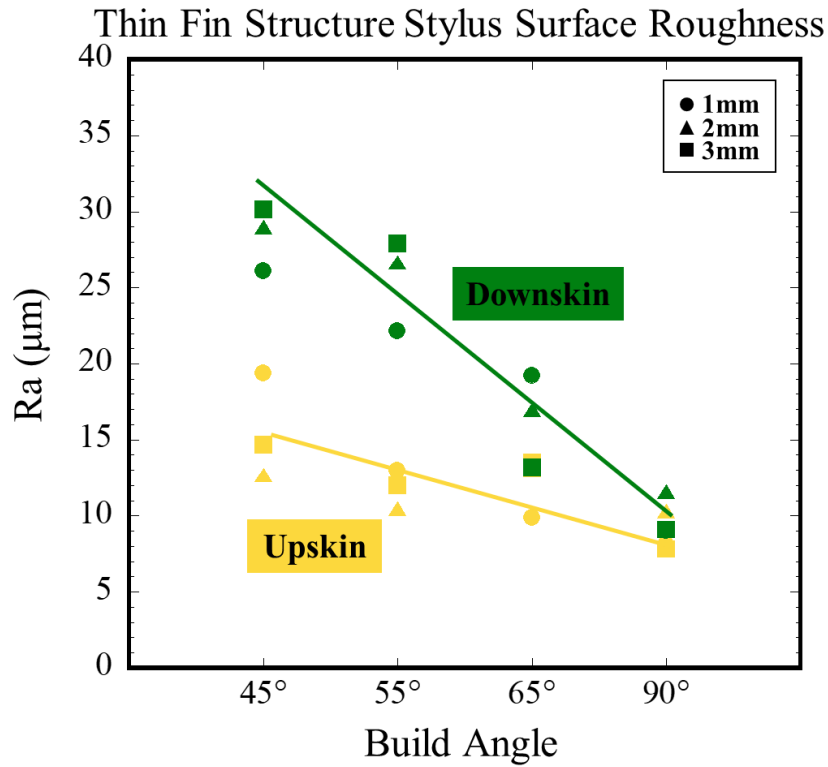


Figure 17. Thin fin structure roughness (by profilometry) as a function of build angle [8].

### 3.2 Vickers Hardness Results

Figure 17 shows the average value for a row of indentations for each thin fin structure, and Figure 18 shows the hardness curves for each row measured.

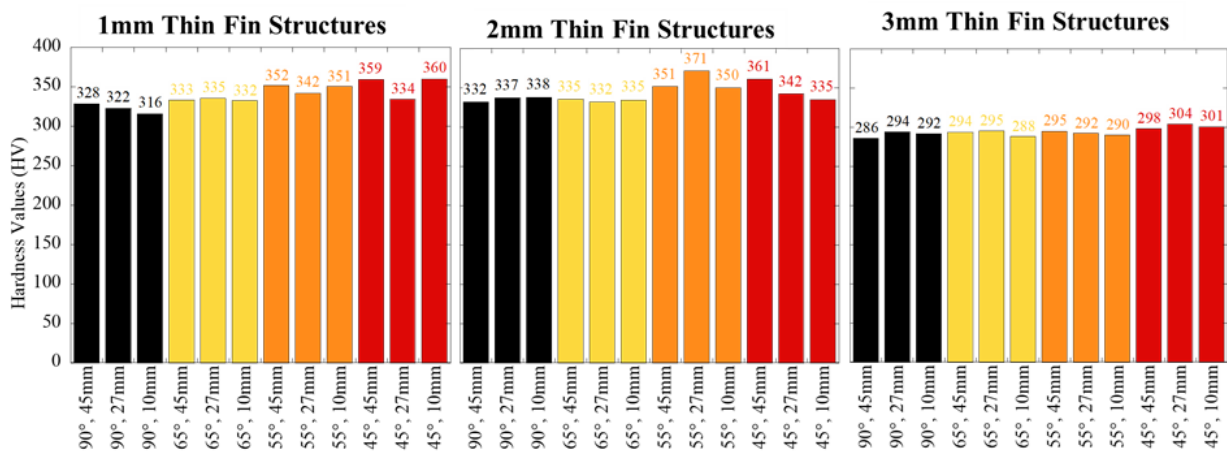


Figure 17. Average indentation row hardness value for each thin fin structure [8].

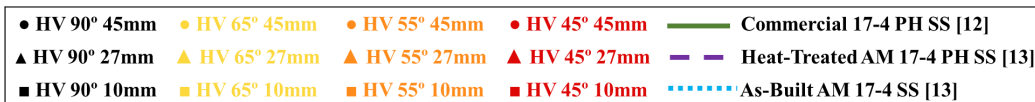
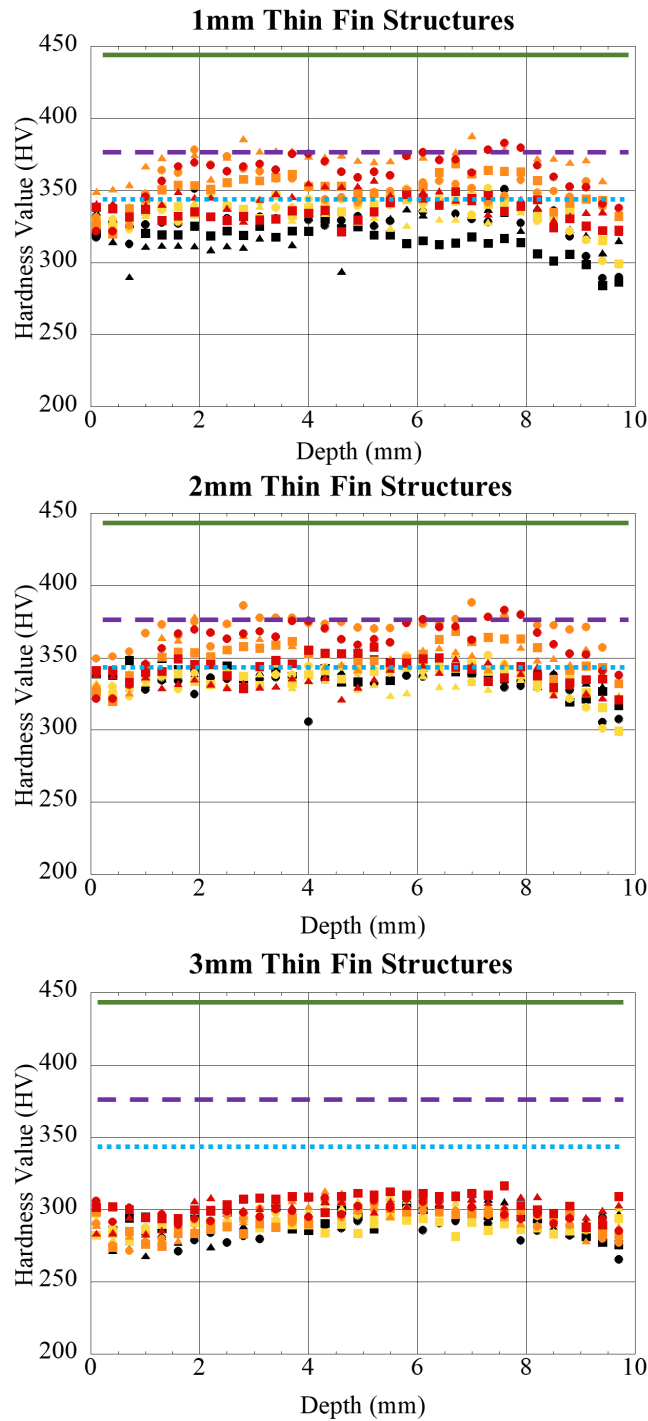


Figure 18. Hardness curves for all thin fin structures [8, 14, 15].

In Figure 18, measured values are compared to the average hardness values of solution-treated and aged commercial 17-4 PH material [14] and both as-built AM 17-4 SS and heat-treated (Condition A and Condition H900) AM 17-4 PH SS material [15].

Hardness does not necessarily vary with respect to height in the build. A decrease in build angle relates to a larger average value and a larger variance in average value for the 1 mm and 2 mm thin fin structures. The 3 mm thin fin structures show similar trends, but at values that are approximately 40 HV lower than the thinner structures. As the thinner structures were polished, they bent due to a stress relief of interior manufacturing residual stresses. The 3 mm structures bent minimally and did not necessitate as much polishing to achieve the desired surface finish, and thus the surface that was tested for the 3 mm thin fins is within the contour pass region. This is reinforced by the decrease in hardness values as the indents approach the free edge of the fin structure, in depths of 9 to 10 mm. Figures 19 and 20 show the zig zag structure hardness data.

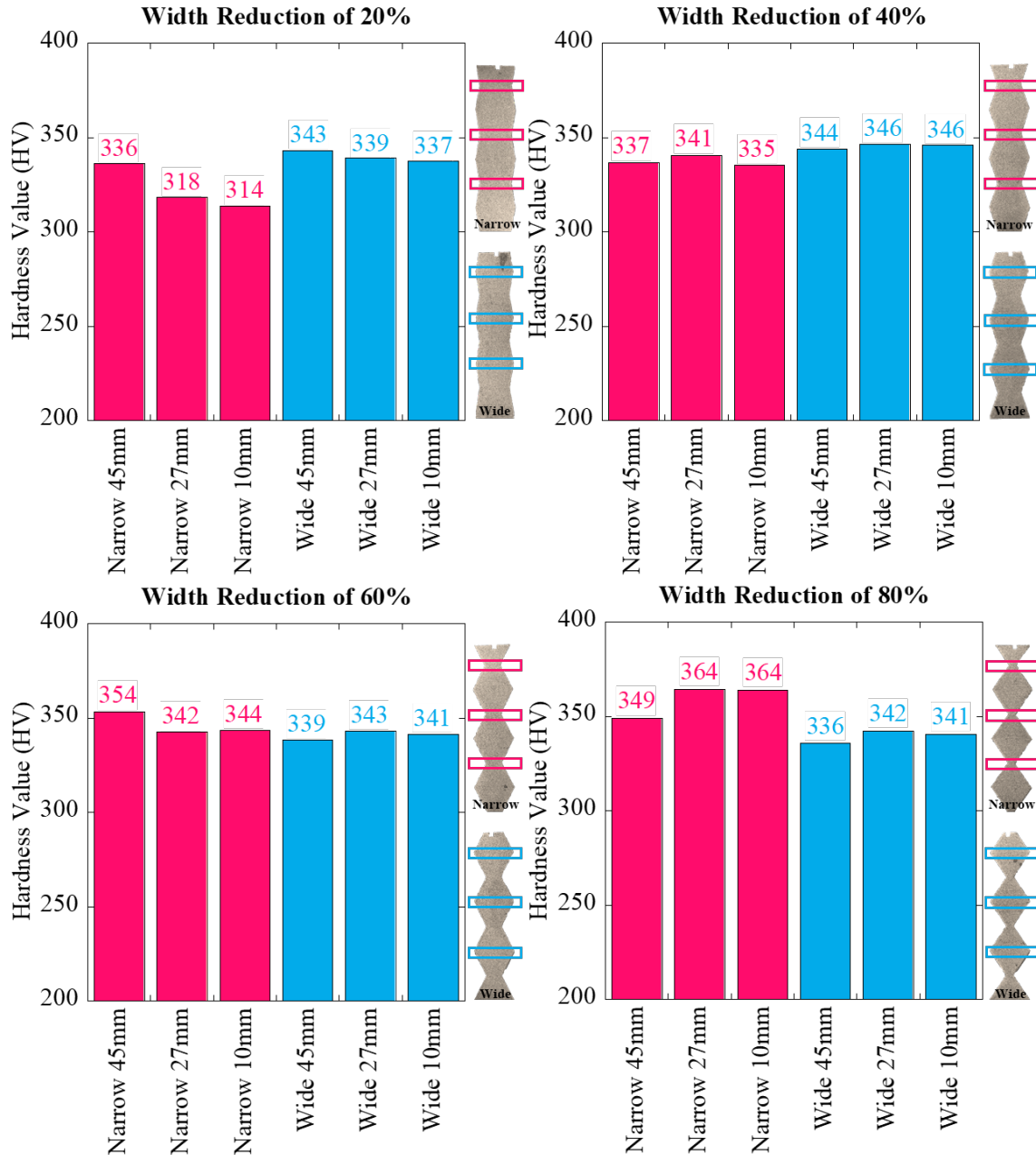


Figure 19. Average indentation row hardness value for each zig zag structure [8].

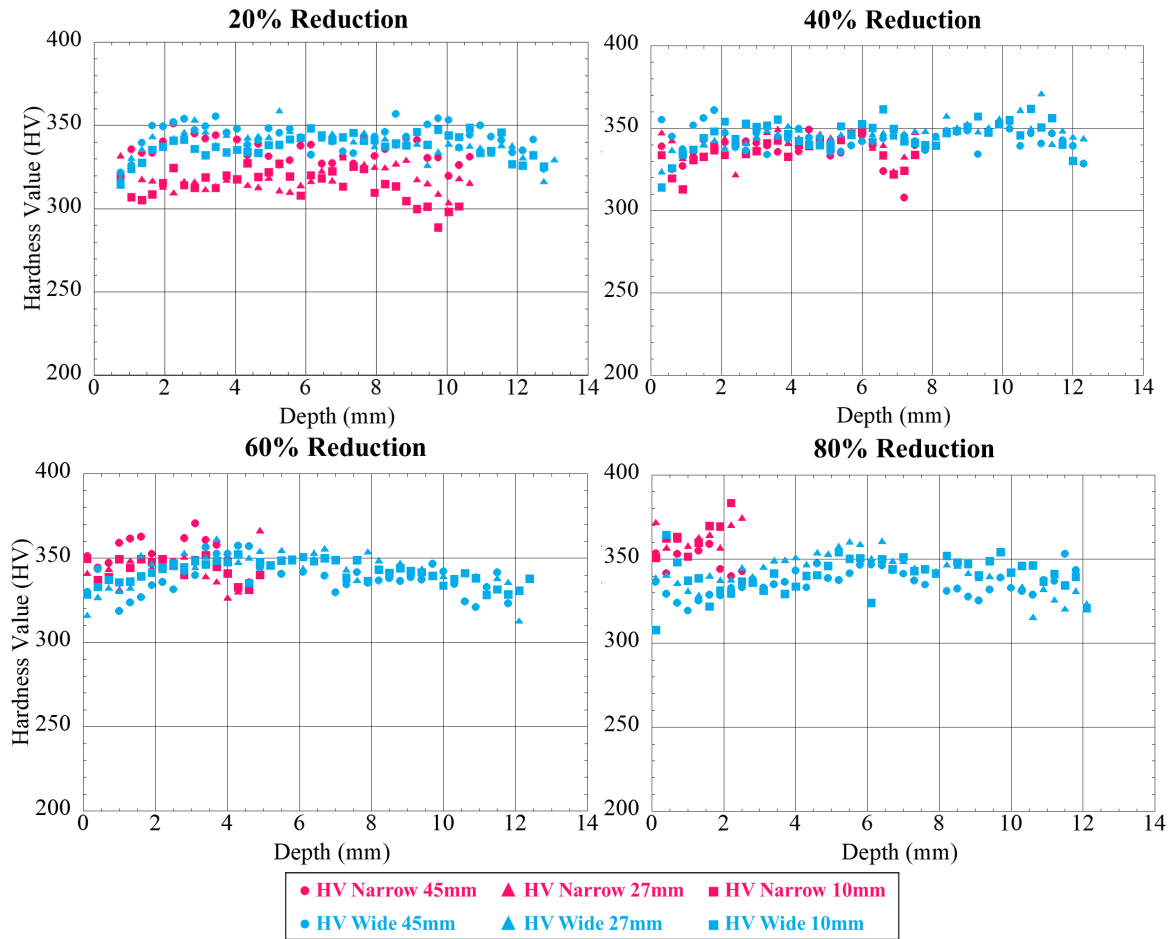


Figure 20. Hardness curves for all zig zag structures [8].

Average hardness values for the narrow base zig zag structures increased with an increase in width reduction. Wide base zig zag structures did not exhibit this response. This suggests that the hardness may vary throughout the height of the zig zag structure build because the locations studied include both the wide and narrow regions of the structure.

#### 4. CONCLUSIONS

From the measurement results for surface roughness and hardness, the following conclusions can be made. There is no clear distinction between surface roughness values across the height or width of a single upskin or downskin surface on a thin fin or zig zag structure, so when measuring those surfaces, measurement location is of little significance. For thin fin structures, the thickness of the actual structure does not impact surface roughness. While optical microscopy provides valuable qualitative imaging, stylus profilometry provides sufficient data and is more productive for operations in the overall repeatability study due to its ease of use and maneuverability.

The differences in hardness values between the 1 mm, 2 mm, and 3 mm thin fin structures is linked to both structure thickness and testing location. The selected location within the depth of a thin fin structure will have an impact on the resulting hardness measurement, and that could be attributed to the cross hatching or residual stress left within the component. Increasing the percentage of width reduction results in increasing hardness values at the reduced region, but hardness values

remain consistent at the widest regions of the structure (15 mm wide), where no width reduction has been applied. Hardness does not necessarily vary with respect to height in a structure that maintains its width.

## 5. REFERENCES

- [1] J. Zhang and Y. Jung. Additive Manufacturing: Materials, Processes, Quantifications and Applications. Butterworth-Heinemann, 2018.
- [2] W. Phillips. Additive Manufacturing: Opportunities, Challenges, Implications. Nova Science Publishers Incorporated, 2016.
- [3] A. Alafaghani, A. Qattawi, and M. Castañón, “Effect of manufacturing parameters on the microstructure and mechanical properties of metal laser sintering parts of precipitate hardenable metals,” *The International Journal of Advanced Manufacturing Technology*, vol. 99, Dec. 2018, doi: 10.1007/s00170-018-2586-5.
- [4] S. Cheruvathur, E. Lass, and C. Campbell, “Additive Manufacturing of 17-4 PH Stainless Steel: Post-processing Heat Treatment to Achieve Uniform Reproducible Microstructure,” *JOM: The Journal of the Minerals, Metals & Materials Society*, vol. 68, Dec. 2015, doi: 10.1007/S11837-015-1754-4.
- [5] A. Kudzal *et al.*, “Effect of scan pattern on the microstructure and mechanical properties of Powder Bed Fusion additive manufactured 17-4 stainless steel,” *Materials & Design*, vol. 133, pp. 205–215, Nov. 2017, doi: 10.1016/j.matdes.2017.07.047.
- [6] S. D. Meredith, J. S. Zuback, J. S. Keist, and T. A. Palmer, “Impact of composition on the heat treatment response of additively manufactured 17–4 PH grade stainless steel,” *Materials Science and Engineering: A*, vol. 738, pp. 44–56, Dec. 2018, doi: 10.1016/j.msea.2018.09.066.
- [7] L. E. Murr *et al.*, “Microstructures and Properties of 17-4 PH Stainless Steel Fabricated by Selective Laser Melting,” *Journal of Materials Research and Technology*, vol. 1, no. 3, pp. 167–177, Oct. 2012, doi: 10.1016/S2238-7854(12)70029-7.
- [8] J. Posey, “Repeatability of Additively Manufactured Precipitation Hardened 17% Chromium – 4% Nickel Stainless Steel,” M.S. thesis, Dept. Mechanical Engineering, UMBC, Baltimore, MD, USA, 2020.
- [9] A. Triantaphyllou *et al.*, “Surface texture measurement for additive manufacturing,” *Surface Topography: Metrology and Properties*, vol. 3, p. 024002, May 2015, doi: 10.1088/2051-672X/3/2/024002.4.2
- [10] “Surftest SJ-210- Series 178-Portable Surface Roughness Tester,” Mitutoyo. <https://ecatalog.mitutoyo.com/Surftest-SJ-210-Series-178-Portable-Surface-Roughness-Tester-C1794.aspx> (accessed Aug. 01, 2020).
- [11] ISO 4288:1996. Geometrical Product Specifications (GPS) — Surface texture: Profile method — Rules and procedures for the assessment of surface texture.

[12] ASTM E92-82(2003), Standard Test Method for Vickers Hardness of Metallic Materials, ASTM International, West Conshohocken, PA, 2003, [www.astm.org](http://www.astm.org)

[13] M. Jafarzadegan, A. Abdollah-zadeh, A. H. Feng, T. Saeid, J. Shen, and H. Assadi, "Microstructure and Mechanical Properties of a Dissimilar Friction Stir Weld between Austenitic Stainless Steel and Low Carbon Steel," *Journal of Materials Science & Technology*, vol. 29, no. 4, pp. 367–372, Apr. 2013, doi: 10.1016/j.jmst.2013.02.008.

[14] M. Mahmoudi, A. Elwany, A. Yadollahi, S. Thompson, L. Bian, and N. Shamsaei, "Mechanical properties and microstructural characterization of selective laser melted 17-4 PH stainless steel," *Rapid Prototyping Journal*, vol. 23, Mar. 2017, doi: 10.1108/RPJ-12-2015-0192.

[15] C.-N. Hsiao, C. S. Chiou, and J.-R. Yang, "Aging reactions in a 17-4 PH stainless steel," *Materials Chemistry and Physics*, vol. 74, pp. 134–142, Mar. 2002, doi: 10.1016/S0254-0584(01)00460-6.